

Tensor-network study of correlation-spreading dynamics in the two-dimensional Bose-Hubbard model

Ryui Kaneko* and Ippei Danshita†

Department of Physics, Kindai University, Higashi-Osaka, Osaka 577-8502, Japan

(Dated: March 23, 2022)

Recent developments in analog quantum simulators based on cold atoms and trapped ions call for cross-validating the accuracy of quantum-simulation experiments with use of quantitative numerical methods; however, it is particularly challenging for dynamics of systems with more than one spatial dimension. Here we demonstrate that a tensor-network method running on classical computers is useful for this purpose. We specifically analyze real-time dynamics of the two-dimensional Bose-Hubbard model after a sudden quench starting from the Mott insulator by means of the tensor-network method based on infinite projected entangled pair states. Calculated single-particle correlation functions are found to be in good agreement with a recent experiment. By estimating the phase and group velocities from the single-particle and density-density correlation functions, we predict how these velocities vary in the moderate interaction region, which serves as a quantitative benchmark for future experiments and numerical simulations.

I. INTRODUCTION

State-of-art experimental platforms of cold atoms and trapped ions as analog quantum simulators have offered unique opportunities for studying far-from-equilibrium dynamics of isolated quantum many-body systems. Thanks to their high controllability and long coherence time, these platforms have already addressed a variety of intriguing phenomena that are in general difficult to simulate with classical computers, such as correlation spreading¹⁻³ and relaxation⁴⁻⁶ after a quantum quench, many-body localization in a disorder potential⁷⁻⁹, and quantum scar states^{10,11}. Nevertheless, accurate numerical methods using classical computers are highly demanded at the current stage of the studies of quantum many-body dynamics, since the classical computation still has complementary advantages over the quantum simulation in that it is free of noise and much more accessible owing to its wide dissemination. In this sense, it is important to cross-check the validity of quantum-simulation experiments and some numerical methods by comparing them with each other.

In particular, direct comparisons between experimental and numerical outputs have been made for dynamical spreading of two-point spatial correlations of the Bose-Hubbard model^{1,3,12-15}, which can be realized experimentally with ultracold bosons in optical lattices¹⁶. The correlation spreading has attracted much theoretical interest^{12-15,17-27} in the sense that it is closely related to fundamental phenomena, including the propagation of quantum information and the thermalization. In one spatial dimension, quasi-exact numerical methods based on matrix product states (MPSs) have been used to validate the performance of the quantum simulators^{1,3,12}. In two dimensions (2D), by contrast, accurate numerical simulations are challenging. Indeed, the comparisons with respect to a single-particle correlation have shown that a few types of the truncated Wigner approximation (TWA) fail to capture the real-time evolution accurately enough to extract the prop-

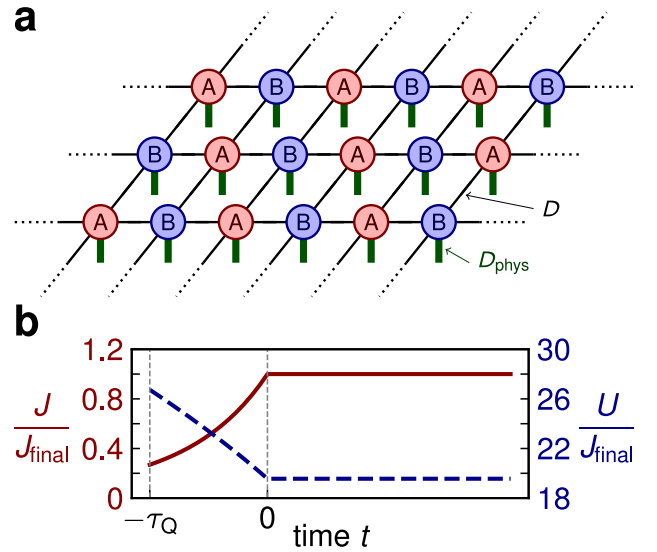


FIG. 1. Setup for numerical simulations of quench dynamics. (a) Schematic figure of infinite projected entangled pair state (iPEPS) with a two-site unit cell. Sublattice sites are represented by A and B. A rank-five tensor at each site is represented as a circle with four thin lines and one thick line. The former lines correspond to the virtual degrees of freedom with the bond dimension D , while the latter line corresponds to the physical degrees of freedom with the dimension of the local Hilbert space D_{phys} . The wave functions become more accurate as D increases. (b) Time dependence of the hopping J (a red solid line) and the onsite interaction U (a blue dashed line) with a finite-time quench. The parameter U/J is varied from ~ 99.4 to ~ 19.6 for $-\tau_Q < t < 0$ with τ_Q being a finite quench time. In the case of a sudden quench, we discard the region $-\tau_Q < t < 0$.

agation velocity of the correlation^{3,14}. Moreover, while the propagation velocities obtained by a two-particle irreducible strong-coupling (2PISC) approach quantitatively agree with the experimental value, and the approach is applicable to much weaker interaction than in the experiment, it does not necessarily provide the exact value of the correlation itself¹⁵.

In this paper, we present quantitative numerical analyses of the correlation-spreading dynamics of the 2D Bose-Hubbard

* rkaneko@phys.kindai.ac.jp

† danshita@phys.kindai.ac.jp

model starting from a Mott insulating initial state with unit filling. To this end, we employ the tensor-network method based on the infinite projected entangled pair state (iPEPS)^{28–35} or the tensor product state^{36–40}, which is an extension of MPS to 2D systems [see Fig.1(a)]. The iPEPS studies on real-time dynamics of isolated^{41–49} and open^{41,42,50–52} quantum systems in 2D have begun very recently. Previous simulations suggest that iPEPS can represent relatively low-entangled states in short-time dynamics for simple spin 1/2 systems^{41–44} and some itinerant electron systems⁴⁶. This observation may be valid for real-time dynamics in Bose-Hubbard systems; however, little is known about it until now. We find that the single-particle correlation computed with iPEPS, as well as the estimated propagation velocity of the correlation front, agrees very well with the experimental result³, demonstrating that iPEPS can be useful for actual quantum-simulation experiments. We also conduct numerical simulations in a moderate interaction region, which has not been addressed by the previous experiments^{1,3}. From the real-time evolution of the single-particle and density-density correlations, we show that the phase and group velocities approach each other when the interaction decreases.

II. RESULTS

A. Model

We consider the Bose-Hubbard model on a square lattice^{53,54}. The Hamiltonian is given as

$$\hat{H} = -J \sum_{\langle ij \rangle} (\hat{a}_i^\dagger \hat{a}_j + \hat{a}_j^\dagger \hat{a}_i) + \frac{U}{2} \sum_i \hat{n}_i (\hat{n}_i - 1) - \mu \sum_i \hat{n}_i, \quad (1)$$

where \hat{a}_i^\dagger and \hat{a}_i are the creation and annihilation operators at site i , $\hat{n}_i = \hat{a}_i^\dagger \hat{a}_i$ is the number operator, J is the strength of the hopping between nearest-neighbor sites, U is the strength of the onsite interaction, and μ is the chemical potential. The notation $\langle ij \rangle$ indicates that sites i and j are nearest neighbors. For simplicity, we ignore the effects of the trap potential and the Gaussian envelopes of optical lattice lasers, which do not affect short-time dynamics. We set the lattice spacing d_{lat} to be unity. The ground state at the commensurate filling is the Mott insulating (superfluid) state for $U \gg J$ ($U \ll J$). Hereafter, we will consider a sudden quench and a quench with a short time [see Fig. 1(b) and Supplementary Note 1 for details].

B. Quench starting from the Mott insulator: Comparison with the exact diagonalization and the experiment

Let us first focus on the case of a sudden quench. We compare our results of iPEPS with those of the exact diagonalization (ED) method and obtain consistent results in a short time. In the ED simulations using the QuSpin library^{55,56}, we choose the system sizes $L_x \times L_y$ up to 5×4 and use the periodic-periodic boundary condition. We examine to what extent the energy is conserved in the iPEPS simulations. The

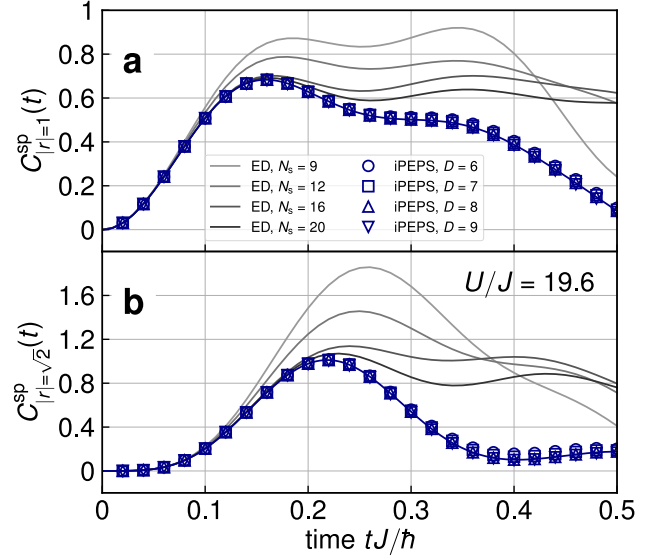


FIG. 2. Single-particle correlation functions $C_r^{\text{SP}}(t)$ in the case of a sudden quench. Comparison is made between the infinite projected entangled pair state algorithm (iPEPS, blue lines with symbols) and the exact diagonalization method (ED, gray lines). The unit of time is taken as the inverse of the strength of the hopping J . U is the strength of the interaction. D is the bond dimension. N_s is the system size. The correlations at distances (a) $|r| = 1$ and (b) $|r| = \sqrt{2}$ are shown. Both results overlap in a short time.

grand potential density $\langle \hat{H} \rangle$ at $T = 0$ starting from the Mott insulator $\otimes_i |n_i = 1\rangle$ should remain constant. They will converge for the bond dimensions $D \geq 6$ and remain nearly constant up to $t \sim 0.4\hbar/J$ (see Supplementary Note 2 for the time dependence of the grand potential density). We also investigate how the single-particle correlations converge with increasing bond dimensions. The equal-time single-particle correlation function at a distance $r = (x, y)$ for the system size N_s is defined as

$$C_r^{\text{SP}}(t) = \frac{1}{2N_s} \sum'_{i,j} \langle \hat{a}_i^\dagger(t) \hat{a}_j(t) + \hat{a}_j^\dagger(t) \hat{a}_i(t) \rangle. \quad (2)$$

Here $\sum'_{i,j}$ denotes the summation over (i, j) that satisfies $|x_j - x_i| = x$ and $|y_j - y_i| = y$. In the iPEPS simulations, $1/N_s \times \sum'_{i,j}$ is replaced by $1/2 \times \sum_{i=A,B} \sum'_j$ with A and B being sublattice sites because of the translational invariance. As shown in Fig. 2, $C_{|r|=1}^{\text{SP}}(t) := [C_{r=(1,0)}^{\text{SP}}(t) + C_{r=(0,1)}^{\text{SP}}(t)]/2$ exhibits a peak at $t \sim 0.15\hbar/J$ in both results, and they overlap in this short time. For $t \gtrsim 0.15\hbar/J$, the correlation functions of ED start to exhibit a significant finite-size effect, whereas those of iPEPS converge for $D \geq 6$. We observe similar behavior for $C_{|r|=\sqrt{2}}^{\text{SP}}(t) := C_{r=(1,1)}^{\text{SP}}(t)$. The iPEPS results are better simulated up to a longer time (see also Supplementary Note 3 for other interaction parameter regions).

Next, we compare the correlations of iPEPS with those of the experiment³ for a finite quench time. In the experiment, a quench to the Mott insulating region has been investigated so far. Figures 3(a–c) show the time evolution of correlations at distances $|r| = 1, 2,$ and 3 , respectively. Qualitative

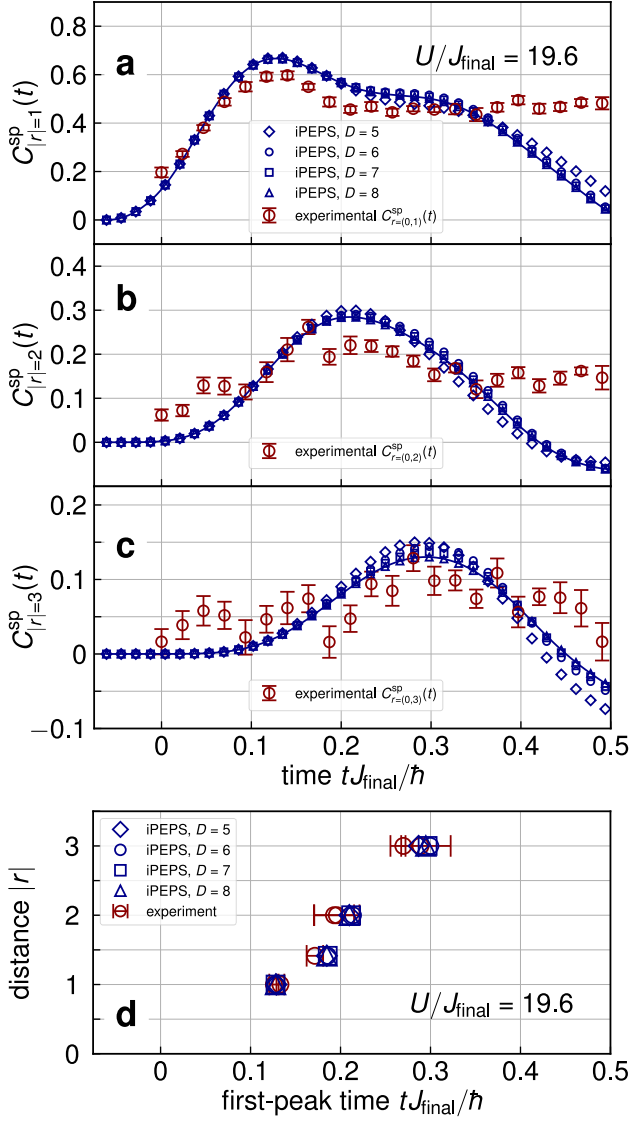


FIG. 3. Single-particle correlation functions $C_r^{\text{sp}}(t)$ in the case of a finite-time quench. Comparison is made between the infinite projected entangled pair state algorithm (iPEPS, blue lines with symbols) and the experiment (red circles with error bars). The unit of time is taken as the inverse of the strength of the hopping J_{final} after the quench. U is the strength of the interaction. D is the bond dimension. The correlations at distances (a) $|r| = 1$, (b) $|r| = 2$, and (c) $|r| = 3$ are shown. The error bars represent the standard error of five independent measurements³. (d) Comparison of the first-peak time between the iPEPS and experimental results. The error bars represent the fitting errors³. The iPEPS and experimental results agree within the experimental errors in all cases.

behavior is essentially equivalent to the case of the sudden quench, although the correlation function shifts to an earlier time. For $|r| = 1$, both data show a peak at $t \sim 0.12\hbar/J_{\text{final}}$. Similarly, the first-peak times are consistent with each other for $|r| = 2$ and 3, and they become longer with increasing distances. When the energy is approximately conserved (namely, for $t \lesssim 0.4\hbar/J_{\text{final}}$, see the time dependence of the grand potential density in Supplementary Note 4), the intensities of

correlations also overlap very well. They are also consistent with those obtained by TWA^{3,13,14}, while the iPEPS simulations can deal with a slightly longer time and capture the correlation peaks more clearly (see also Supplementary Note 5 for a detailed comparison with the TWA results). To see how well they match more quantitatively, we also compare the first-peak position of iPEPS with that of the experiment³ as shown in Fig. 3(d). Both iPEPS and experimental results agree very well.

C. Estimates of group and phase velocities in the moderate interaction region

Having confirmed the applicability of iPEPS simulations to real-time evolution of the Bose-Hubbard model, we study how information propagates by a sudden quench in the moderate interaction region. There are two kinds of velocity that are relevant to the correlation spreading. One is the group velocity v_{gr} , which corresponds to the propagation of the envelope of the wave packet and is a suitable quantity to characterize the spreading of correlations. In non-relativistic quantum many-body systems, v_{gr} is bounded above, and the upper bound is known as the Lieb-Robinson bound^{23–27,57,58}. Notice that the Lieb-Robinson bound for the Bose-Hubbard model has not been rigorously derived with a few exceptions for limited situations^{18,23–27}. The phase velocity v_{ph} is the other characteristic quantity, which corresponds to the propagation of the first peak of the wave packet, and does not have to obey the Lieb-Robinson bound.

Although the exact Lieb-Robinson bound is not known for the Bose-Hubbard model, there are some values that can be used as a guide. As discussed in previous studies^{1,3,12} in the weak interaction region, the single-particle dispersion up to constant is approximately given as $\epsilon_{U \ll J}(\mathbf{k}) \sim -2J \sum_{\alpha} \cos k_{\alpha}$ ($\alpha = x, y$ in 2D), which is equivalent to the dispersion of free particles. The velocity of the correlation spreading would be well characterized by the group velocity of the single-particle excitation. The largest velocity of a single quasiparticle (along the horizontal or vertical direction α) is described by the maximal slope of the dispersion and is given by $v = \max_{k_{\alpha}} [d|\epsilon_{U \ll J}(\mathbf{k})|/dk_{\alpha}]/\hbar = 2J/\hbar$. Because both doublon and holon quasiparticles propagate with the group velocity v , the front of the correlation function moves at the speed of v_{front} , which should be smaller than $v_{\text{max}} = 2v = 4J/\hbar$. Therefore, this speed v_{max} can be regarded as the Lieb-Robinson-bound-like value. Likewise, in the strong interaction region, the doublon and holon dispersions up to constant are approximately given as $\epsilon_{U \gg J}^{(d)}(\mathbf{k}) \sim -4J \sum_{\alpha} \cos k_{\alpha}$ and $\epsilon_{U \gg J}^{(h)}(-\mathbf{k}) \sim -2J \sum_{\alpha} \cos k_{\alpha}$, respectively. Because the doublons and holons propagate with respective velocities $4J/\hbar$ and $2J/\hbar$, v_{front} should be smaller than these two sum $v_{\text{max}} = 6J/\hbar$. Although we know the approximate limit values, the intermediate interaction region is yet to be explored.

To estimate the group velocity from the single-particle correlations, long-time simulations are required in general. However, it is challenging in the iPEPS simulations. To circumvent the difficulty, we estimate the group velocity by the density-

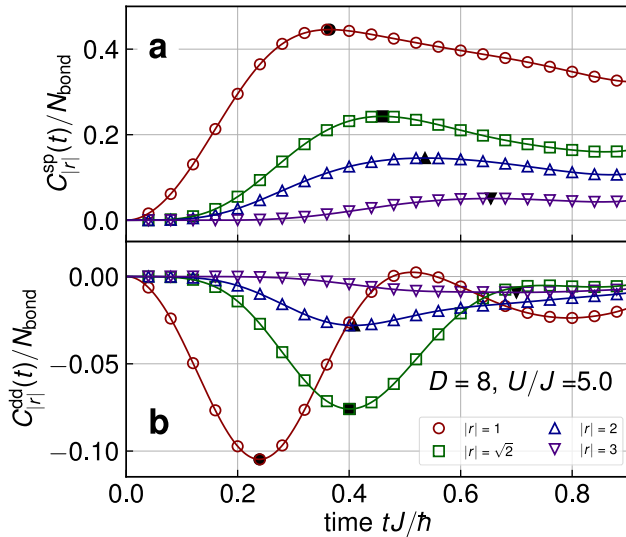


FIG. 4. Single particle and density-density correlation functions used to extract the propagation velocities. (a) Single-particle [$C_r^{\text{sp}}(t)$] and (b) density-density [$C_r^{\text{dd}}(t)$] correlation functions per bond at the interaction strength $U/J = 5$ for the bond dimension $D = 8$. The unit of time is taken as the inverse of the strength of the hopping J . The normalization factor at a distance $\mathbf{r} = (x, y)$ is given as $N_{\text{bond}} = 2$ for $x \neq y$ ($|\mathbf{r}| = 1, 2$, and 3), while it is $N_{\text{bond}} = 4$ for $x = y$ ($|\mathbf{r}| = \sqrt{2}$). The black symbol corresponds to the first peak in the correlation function obtained by cubic spline interpolation of data points. The propagation velocities along the horizontal or vertical axis are extracted by the data at $|\mathbf{r}| = 1, 2$, and 3 . The velocity estimated from the density-density correlation functions is slower than that from the single-particle correlation functions.

density correlation. It is known that the propagation velocity of the first peak of this correlation agrees very well with the group velocity^{1,12}. The equal-time density-density correlation function at a distance $\mathbf{r} = (x, y)$ for the system size N_s is defined as

$$C_{\mathbf{r}}^{\text{dd}}(t) = \frac{1}{N_s} \sum'_{i,j} \langle \hat{n}_i(t) \hat{n}_j(t) \rangle_c, \quad (3)$$

where $\langle \dots \rangle_c$ denotes a connected correlation function. In our simulations, $\langle \hat{n}_i(t) \hat{n}_j(t) \rangle_c = \langle \hat{n}_i(t) \hat{n}_j(t) \rangle - 1$ because $\langle \hat{n}_i(t) \rangle = 1$ for all sites and time steps. As in $C_{\mathbf{r}}^{\text{sp}}(t)$, the summation is replaced by that within sublattice sites in the iPEPS simulations. The parity-parity correlation closely related to the density-density one can be measured in experiments by using the quantum-gas microscope techniques¹.

We extract the propagation velocities from the first peak in both correlations for $|\mathbf{r}| = 1, 2$, and 3 . For simplicity, we consider the sudden quench hereafter. When the interaction becomes weaker, we have confirmed that the energy is conserved in a longer time frame; typically, $t \leq 0.9\hbar/J$ for $U/J \sim 5$ (see Supplementary Note 6 for the time dependence of the grand potential density in the weaker interaction region). All the correlation peaks for $|\mathbf{r}| \leq 3$ appear in this time frame (see Fig. 4). The first peak of the single-particle correlation appears at $t \sim 0.35\hbar/J$ for $|\mathbf{r}| = 1$, while it appears at $t \sim 0.65\hbar/J$ for $|\mathbf{r}| = 3$. By contrast, the first peak

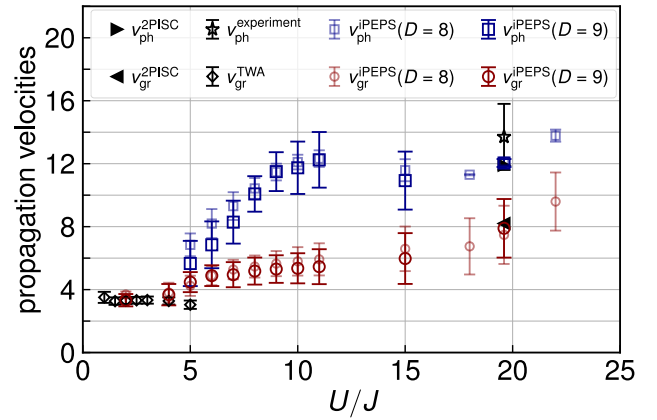


FIG. 5. Propagation velocities as functions of the ratio between the interaction (U) and hopping (J) strengths. The group (v_{gr} , red circles) and phase (v_{ph} , blue squares) velocities are estimated from the density-density and single-particle correlation functions for the bond dimensions $D = 8$ and $D = 9$ using the infinite projected entangled pair state (iPEPS) algorithm. The data for $D = 8$ and $D = 9$ overlap within the error bars. The velocities and their error bars are obtained by extrapolation of the distance dependence of the peak time. The results obtained by the two-particle irreducible strong-coupling (2PISC) approach¹⁵ (triangles), the truncated Wigner approximation (TWA)¹³ (diamonds), and the experiment³ (a star) are shown. Both velocities gradually merge with decreasing interaction.

of the density-density correlation appears at $t \sim 0.25\hbar/J$ for $|\mathbf{r}| = 1$, while it appears at $t \sim 0.7\hbar/J$ for $|\mathbf{r}| = 3$. It takes a long time for propagation in the latter case. (See also the correlations for other interaction parameters given in Supplementary Note 7. Extraction of propagation velocities in the intermediate and strong interaction regions is summarized in Supplementary Notes 8 and 9, respectively.) The first-peak time is almost a linear function of the distance, and the system exhibits the light-cone-like spreading of correlations (see the time dependence of distance summarized in Supplementary Note 8).

We summarize the interaction dependence of the group and phase velocities in Fig. 5. In the weak interaction region, the estimated group velocities are $v_{\text{gr}} \sim 4J/\hbar$. They are similar to those obtained by the TWA at filling factor $\nu = 10$ ¹³. They are also consistent with the group velocity $v_{\text{gr}}(U = 0) = 4J/\hbar$ of a single particle¹³. In the strong interaction region, the estimated group velocity $v_{\text{gr}} \sim (8 \pm 2)J/\hbar$ at $U/J = 19.6$ coincides with that obtained by the 2PISC approach¹⁵ within the error bar of extrapolation. It is also comparable to the group velocity $v_{\text{gr}}(U \gg J) = 6J/\hbar \times [1 + O(J^2/U^2)]$ of a quasi-particle in the large U limit^{1,3,12}. Similarly, the estimated phase velocity agrees very well with the results of the 2PISC approach¹⁵ and the experiment³. In the intermediate region, the estimated group velocity is closer to the single-particle group velocity in the superfluid region, whereas it is comparable to the 2PISC result near and above the critical point $U_c/J \sim 16.7$ ^{59–61}.

In all parameter regions, no anomalies appear in the propagation velocities. As for the real-time dynamics after a sudden quench, there is no sign of the superfluid-Mott insulator

quantum phase transition. This is because non-universal high-energy excitations come into play during the time evolution. The quantum phase transition at zero temperature does not have to affect the time-evolved states.

Both group and phase velocities gradually converge to the same value as U/J is decreased. This phenomenon can be understood in terms of the separation of the energy scales. When the interaction U is much stronger than the hopping J , the correlation function oscillates rapidly as a function of time^{12,22}. The correlation function exhibits the envelope of the wave packet. The time scale of the period of oscillation is $\sim 1/U$, which determines the phase velocity $v_{\text{ph}} \sim U$. On the other hand, the time scale of the period of the envelope is $\sim 1/J$, which determines the group velocity $v_{\text{gr}} \sim J$. Hence, the group and phase velocities differ as long as $U \gg J$. When the interaction U becomes comparable to the hopping J , they start to coincide by slowing down the vibration. Note that this phenomenon occurs irrespective of the presence or absence of phase transitions.

III. CONCLUSIONS

We have studied real-time dynamics of the 2D Bose-Hubbard model after a sudden quench starting from the Mott insulator with unit filling. We have employed the 2D tensor-network method based on the iPEPSs, which are the 2D extension of the well-known MPSs in one dimension. Calculated single-particle correlation functions reproduce the recent experimental results very well. The iPEPS algorithm can simulate real-time dynamics long enough for extracting the propagation velocities from correlations. This fact suggests that, for the quench dynamics starting from the Mott insulator in the 2D Bose-Hubbard model, time-evolved states are not so highly entangled before and even slightly after the time at which the correlation front is reached. This finding raises questions about our understanding of how quantum states get entangled with real-time evolution.

We have also estimated the group and phase velocities in the moderate interaction region, in which the 2PISC approach and the TWA are not applicable. The estimated group velocities are continuously connected without singularity in the middle. Our findings would be useful in the future analog quantum simulation and in the future examination of the rigorous Lieb-Robinson bound of Bose-Hubbard systems. The ability of the tensor-network method that accurately calculates the real-time dynamics of 2D quantum many-body systems opens up the possibility of applying it to other quantum-simulation platforms, such as Rydberg atoms, trapped ions, and superconducting circuits.

IV. METHODS

A. Real-time evolution by infinite projected entangled pair states

We prepare iPEPS with a two-site unit cell [see Fig. 1(a)]. The symbols D and D_{phys} denote the virtual bond dimension and the dimension of the local Hilbert space, respectively. The former improves the accuracy of the wave function, whereas the latter corresponds to the maximum particle number n_{max} as $D_{\text{phys}} = n_{\text{max}} + 1$. Although n_{max} can take infinity in Bose-Hubbard systems, it is practically bounded above in the presence of interaction^{62,63}. We can choose finite D_{phys} in the simulations of real-time dynamics. In the case of a sudden quench to the Mott insulating region ($U/J > U_c/J \sim 16.7$ ⁵⁹⁻⁶¹), we set the dimension of the local Hilbert space as $D_{\text{phys}} = 3$ because the number of particles deviates only slightly from unity^{62,63}. For $U/J < U_c/J$, we choose $D_{\text{phys}} = 5$ so that the wave functions can further take into account the effect of particle fluctuations. When U is close to zero (at $U/J = 2$ in our simulations), we use slightly larger $D_{\text{phys}} = 7$ (see Supplementary Note 10 for the details of the choice of the dimensions of the local Hilbert space). The initial Mott insulating state $\otimes_i |n_i = 1\rangle$ can be represented with the bond dimension $D = 1$. As for static properties, the Bose-Hubbard model was investigated by finite PEPS or iPEPS, and the phase transition between the Mott insulating and superfluid phases was reproduced⁶⁴⁻⁷².

The wave function at each time $|\Psi(t)\rangle = e^{-it\hat{H}/\hbar}|\Psi(0)\rangle$ is obtained by real-time evolving iPEPS⁴¹⁻⁴³. The real-time evolution operator in a small time step dt can be approximated by the Suzuki-Trotter decomposition⁷³⁻⁷⁵ as $e^{-idt\hat{H}/\hbar} \sim \prod_{\langle ij \rangle} e^{-idt\hat{H}_{ij}/\hbar}$, where $\hat{H}_{ij} = -J(\hat{a}_i^\dagger \hat{a}_j + \hat{a}_j^\dagger \hat{a}_i) + U[\hat{n}_i(\hat{n}_i - 1) + \hat{n}_j(\hat{n}_j - 1)] / (2z) - \mu(\hat{n}_i + \hat{n}_j) / z$ with the coordination number $z = 4$ is the local Hamiltonian satisfying $\hat{H} = \sum_{\langle ij \rangle} \hat{H}_{ij}$. After applying the two-site gate $e^{-idt\hat{H}_{ij}/\hbar}$ to neighboring tensors, we approximate the local tensors by the singular value decomposition in such a way that the virtual bond dimension of iPEPS remains D . In the actual simulations, the second-order Suzuki-Trotter decomposition is used for this simple update algorithm^{32,76}, and the tensor-network library TeNeS⁷⁷⁻⁷⁹ is adopted. The wave functions are optimized up to the bond dimension $D = 9$. Qualitative behavior of correlation functions is found to be nearly the same for $D \geq 6$. When extracting the propagation velocities, we mainly use the data for $D = 8$ and $D = 9$ to ensure sufficient convergence of physical quantities. We do not preserve the $U(1)$ symmetry during the calculation. Even without respecting the symmetry, we have numerically found that at these values of D , the number of particles is nearly conserved during the real-time evolution starting from the Mott insulator.

Physical quantities in the thermodynamic limit are calculated by the corner transfer matrix renormalization group (CTMRG) method^{33-35,37,80-86}. The bond dimension of the environment tensors is chosen as $\chi = 2D^2$ to ensure that physical quantities are well converged.

To compare our results obtained by iPEPS with the experiment³, we consider a quench with a short time $\tau_Q = 0.1 \text{ ms}$ ^{13,14}

[see Fig. 1(b)]. For $-\tau_Q < t < 0$, both J and U are controlled. The wave function is updated as $|\Psi(t + dt)\rangle \sim e^{-idt\hat{H}(t)/\hbar}|\Psi(t)\rangle$ with the time-dependent Hamiltonian $\hat{H}(t)$ in this region. For $t > 0$, both parameters are fixed. We take $J_{\text{final}} = J(t = 0) \sim 0.0612\hbar/\tau_Q$ as the unit of energy. The discrete time step for the real-time evolution is set to be $dt/(\hbar/J_{\text{final}}) = \tau_Q/(\hbar/J_{\text{final}})/15 \sim 0.00408$ for all t . To compare the iPEPS results with the exact real-time dynamics in finite-size systems, we also consider a sudden parameter change and set the time step as $dt/(\hbar/J) = 0.005$. We have checked that the simulations with doubled and halved dt do not change the results significantly.

VI. DATA AVAILABILITY

The data obtained by the iPEPS and ED simulations in this paper are available at <https://doi.org/10.5281/zenodo.6085592>. The experimental data³ and the data obtained by the TWA simulations¹³ in this paper are available from the authors upon request.

VI. CODE AVAILABILITY

The codes in this paper are available from the authors upon request.

REFERENCES

- [1] M. Cheneau, P. Barmettler, D. Poletti, M. Endres, P. Schauß, T. Fukuhara, C. Gross, I. Bloch, C. Kollath, and S. Kuhr, *Light-cone-like spreading of correlations in a quantum many-body system*, *Nature* **481**, 484 (2012).
- [2] P. Jurcevic, B. P. Lanyon, P. Hauke, C. Hempel, P. Zoller, R. Blatt, and C. F. Roos, *Quasiparticle engineering and entanglement propagation in a quantum many-body system*, *Nature* **511**, 202 (2014).
- [3] Y. Takasu, T. Yagami, H. Asaka, Y. Fukushima, K. Nagao, S. Goto, I. Danshita, and Y. Takahashi, *Energy redistribution and spatio-temporal evolution of correlations after a sudden quench of the Bose-Hubbard model*, *Sci. Adv.* **6**, eaba9255 (2020).
- [4] S. Trotzky, Y.-A. Chen, A. Flesch, I. P. McCulloch, U. Schollwöck, J. Eisert, and I. Bloch, *Probing the relaxation towards equilibrium in an isolated strongly correlated one-dimensional Bose gas*, *Nat. Phys.* **8**, 325 (2012).
- [5] T. Langen, S. Erne, R. Geiger, B. Rauer, T. Schweigler, M. Kuhnert, W. Rohringer, I. E. Mazets, T. Gasenzer, and J. Schmiedmayer, *Experimental observation of a generalized Gibbs ensemble*, *Science* **348**, 207 (2015).
- [6] A. M. Kaufman, M. E. Tai, A. Lukin, M. Rispoli, R. Schittko, P. M. Preiss, and M. Greiner, *Quantum thermalization through entanglement in an isolated many-body system*, *Science* **353**, 794 (2016).
- [7] M. Schreiber, S. S. Hodgman, P. Bordia, H. P. Lüschen, M. H. Fischer, R. Vosk, E. Altman, U. Schneider, and I. Bloch, *Observation of many-body localization of interacting fermions in a quasirandom optical lattice*, *Science* **349**, 842 (2015).
- [8] J.-y. Choi, S. Hild, J. Zeiher, P. Schauß, A. Rubio-Abadal, T. Yefsah, V. Khemani, D. A. Huse, I. Bloch, and C. Gross, *Exploring the many-body localization transition in two dimensions*, *Science* **352**, 1547 (2016).
- [9] J. Smith, A. Lee, P. Richerme, B. Neyenhuis, P. W. Hess, P. Hauke, M. Heyl, D. A. Huse, and C. Monroe, *Many-body localization in a quantum simulator with programmable random disorder*, *Nat. Phys.* **12**, 907 (2016).
- [10] H. Bernien, S. Schwartz, A. Keesling, H. Levine, A. Omran, H. Pichler, S. Choi, A. S. Zibrov, M. Endres, M. Greiner, V. Vuletić, and M. D. Lukin, *Probing many-body dynamics on a 51-atom quantum simulator*, *Nature* **551**, 579 (2017).
- [11] C. J. Turner, A. A. Michailidis, D. A. Abanin, M. Serbyn, and Z. Papić, *Weak ergodicity breaking from quantum many-body scars*, *Nat. Phys.* **14**, 745 (2018).
- [12] P. Barmettler, D. Poletti, M. Cheneau, and C. Kollath, *Propagation front of correlations in an interacting Bose gas*, *Phys. Rev. A* **85**, 053625 (2012).
- [13] K. Nagao, M. Kunimi, Y. Takasu, Y. Takahashi, and I. Danshita, *Semiclassical quench dynamics of Bose gases in optical lattices*, *Phys. Rev. A* **99**, 023622 (2019).
- [14] K. Nagao, Y. Takasu, Y. Takahashi, and I. Danshita, *SU(3) truncated Wigner approximation for strongly interacting Bose gases*, *Phys. Rev. Research* **3**, 043091 (2021).
- [15] A. Mokhtari-Jazi, M. R. C. Fitzpatrick, and M. P. Kennett, *Phase and group velocities for correlation spreading in the Mott phase of the Bose-Hubbard model in dimensions greater than one*, *Phys. Rev. A* **103**, 023334 (2021).
- [16] M. Greiner, O. Mandel, T. Esslinger, T. W. Hänsch, and I. Bloch, *Quantum phase transition from a superfluid to a Mott insulator in a gas of ultracold atoms*, *Nature* **415**, 39 (2002).
- [17] A. M. Läuchli and C. Kollath, *Spreading of correlations and entanglement after a quench in the one-dimensional Bose-Hubbard model*, *J. Stat. Mech. Theory Exp.* **2008**, P05018 (2008).
- [18] N. Schuch, S. K. Harrison, T. J. Osborne, and J. Eisert, *Information propagation for interacting-particle systems*, *Phys. Rev. A* **84**, 032309 (2011).
- [19] G. Carleo, F. Becca, L. Sanchez-Palencia, S. Sorella, and M. Fabrizio, *Light-cone effect and supersonic correlations in one- and two-dimensional bosonic superfluids*, *Phys. Rev. A* **89**, 031602(R) (2014).
- [20] L. Cevolani, J. Despres, G. Carleo, L. Tagliacozzo, and L. Sanchez-Palencia, *Universal scaling laws for correlation spreading in quantum systems with short- and long-range interactions*, *Phys. Rev. B* **98**, 024302 (2018).
- [21] M. R. C. Fitzpatrick and M. P. Kennett, *Light-cone-like spreading of single-particle correlations in the Bose-Hubbard model after a quantum quench in the strong-coupling regime*, *Phys. Rev. A* **98**, 053618 (2018).
- [22] J. Despres, L. Villa, and L. Sanchez-Palencia, *Twofold correlation spreading in a strongly correlated lattice Bose gas*, *Sci. Rep.* **9**, 4135 (2019).
- [23] Z. Wang and K. R. A. Hazzard, *Tightening the Lieb-Robinson Bound in Locally Interacting Systems*, *PRX Quantum* **1**, 010303 (2020).
- [24] T. Kuwahara and K. Saito, *Lieb-Robinson Bound and Almost-Linear Light Cone in Interacting Boson Systems*, *Phys. Rev. Lett.* **127**, 070403 (2021).
- [25] C. Yin and A. Lucas, *Finite speed of quantum information in models of interacting bosons at finite density*, [arXiv:2106.09726](https://arxiv.org/abs/2106.09726).

- [26] J. Faupin, M. Lemm, and I. M. Sigal, *On Lieb-Robinson bounds for the Bose-Hubbard model*, [arXiv:2109.04103](#).
- [27] J. Faupin, M. Lemm, and I. M. Sigal, *Maximal speed for macroscopic particle transport in the Bose-Hubbard model*, [arXiv:2110.04313](#).
- [28] M. A. Martín-Delgado, M. Roncaglia, and G. Sierra, *Stripe ansätze from exactly solved models*, *Phys. Rev. B* **64**, 075117 (2001).
- [29] F. Verstraete and J. I. Cirac, *Renormalization algorithms for quantum-many body systems in two and higher dimensions*, [arXiv:cond-mat/0407066](#).
- [30] F. Verstraete and J. I. Cirac, *Valence-bond states for quantum computation*, *Phys. Rev. A* **70**, 060302(R) (2004).
- [31] F. Verstraete, V. Murg, and J. I. Cirac, *Matrix product states, projected entangled pair states, and variational renormalization group methods for quantum spin systems*, *Adv. Phys.* **57**, 143 (2008).
- [32] J. Jordan, R. Orús, G. Vidal, F. Verstraete, and J. I. Cirac, *Classical Simulation of Infinite-Size Quantum Lattice Systems in Two Spatial Dimensions*, *Phys. Rev. Lett.* **101**, 250602 (2008).
- [33] H. N. Phien, J. A. Bengua, H. D. Tuan, P. Corboz, and R. Orús, *Infinite projected entangled pair states algorithm improved: Fast full update and gauge fixing*, *Phys. Rev. B* **92**, 035142 (2015).
- [34] R. Orús, *A practical introduction to tensor networks: Matrix product states and projected entangled pair states*, *Ann. Phys. (N.Y.)* **349**, 117 (2014).
- [35] R. Orús, *Tensor networks for complex quantum systems*, *Nat. Rev. Phys.* **1**, 538 (2019).
- [36] Y. Heida, K. Okunishi, and Y. Akutsu, *Numerical renormalization approach to two-dimensional quantum antiferromagnets with valence-bond-solid type ground state*, *New J. Phys.* **1**, 7 (1999).
- [37] K. Okunishi and T. Nishino, *Kramers-Wannier approximation for the 3D Ising model*, *Prog. Theor. Phys.* **103**, 541 (2000).
- [38] T. Nishino, Y. Heida, K. Okunishi, N. Maeshima, Y. Akutsu, and A. Gendiar, *Two-dimensional tensor product variational formulation*, *Prog. Theor. Phys.* **105**, 409 (2001).
- [39] N. Maeshima, Y. Heida, Y. Akutsu, T. Nishino, and K. Okunishi, *Vertical density matrix algorithm: A higher-dimensional numerical renormalization scheme based on the tensor product state ansatz*, *Phys. Rev. E* **64**, 016705 (2001).
- [40] Y. Nishio, N. Maeshima, A. Gendiar, and T. Nishino, *Tensor product variational formulation for quantum systems*, [arXiv:cond-mat/0401115](#).
- [41] A. Kshetrimayum, H. Weimer, and R. Orús, *A simple tensor network algorithm for two-dimensional steady states*, *Nat. Commun.* **8**, 1 (2017).
- [42] P. Czarnik, J. Dziarmaga, and P. Corboz, *Time evolution of an infinite projected entangled pair state: An efficient algorithm*, *Phys. Rev. B* **99**, 035115 (2019).
- [43] C. Hubig and J. I. Cirac, *Time-dependent study of disordered models with infinite projected entangled pair states*, *SciPost Phys.* **6**, 31 (2019).
- [44] A. Kshetrimayum, M. Goihl, and J. Eisert, *Time evolution of many-body localized systems in two spatial dimensions*, *Phys. Rev. B* **102**, 235132 (2020).
- [45] A. Kshetrimayum, M. Goihl, D. M. Kennes, and J. Eisert, *Quantum time crystals with programmable disorder in higher dimensions*, *Phys. Rev. B* **103**, 224205 (2021).
- [46] C. Hubig, A. Bohrdt, M. Knap, F. Grusdt, and J. I. Cirac, *Evaluation of time-dependent correlators after a local quench in iPEPS: hole motion in the t-J model*, *SciPost Phys.* **8**, 21 (2020).
- [47] A. M. Alhambra and J. I. Cirac, *Locally Accurate Tensor Networks for Thermal States and Time Evolution*, *PRX Quantum* **2**, 040331 (2021).
- [48] M. Schmitt, M. M. Rams, J. Dziarmaga, M. Heyl, and W. H. Zurek, *Quantum phase transition dynamics in the two-dimensional transverse-field Ising model*, [arXiv:2106.09046](#).
- [49] J. Dziarmaga, *Time evolution of an infinite projected entangled pair state: Neighborhood tensor update*, *Phys. Rev. B* **104**, 094411 (2021).
- [50] H. Weimer, A. Kshetrimayum, and R. Orús, *Simulation methods for open quantum many-body systems*, *Rev. Mod. Phys.* **93**, 015008 (2021).
- [51] C. Mc Keever and M. H. Szymańska, *Stable iPEPO Tensor-Network Algorithm for Dynamics of Two-Dimensional Open Quantum Lattice Models*, *Phys. Rev. X* **11**, 021035 (2021).
- [52] D. Kilda, A. Biella, M. Schiro, R. Fazio, and J. Keeling, *On the stability of the infinite Projected Entangled Pair Operator ansatz for driven-dissipative 2D lattices*, *SciPost Phys. Core* **4**, 5 (2021).
- [53] M. P. A. Fisher, P. B. Weichman, G. Grinstein, and D. S. Fisher, *Boson localization and the superfluid-insulator transition*, *Phys. Rev. B* **40**, 546 (1989).
- [54] D. Jaksch, C. Bruder, J. I. Cirac, C. W. Gardiner, and P. Zoller, *Cold Bosonic Atoms in Optical Lattices*, *Phys. Rev. Lett.* **81**, 3108 (1998).
- [55] P. Weinberg and M. Bukov, *QuSpin: a Python Package for Dynamics and Exact Diagonalisation of Quantum Many Body Systems part I: spin chains*, *SciPost Phys.* **2**, 003 (2017).
- [56] P. Weinberg and M. Bukov, *QuSpin: a Python Package for Dynamics and Exact Diagonalisation of Quantum Many Body Systems. Part II: bosons, fermions and higher spins*, *SciPost Phys.* **7**, 20 (2019).
- [57] E. H. Lieb and D. W. Robinson, *The finite group velocity of quantum spin systems*, *Commun. Math. Phys.* **28**, 251 (1972).
- [58] M. B. Hastings, *Locality in Quantum Systems*, [arXiv:1008.5137](#).
- [59] N. Elstner and H. Monien, *Dynamics and thermodynamics of the Bose-Hubbard model*, *Phys. Rev. B* **59**, 12184 (1999).
- [60] B. Capogrosso-Sansone, Ş. G. Söyler, N. Prokof'ev, and B. Svistunov, *Monte Carlo study of the two-dimensional Bose-Hubbard model*, *Phys. Rev. A* **77**, 015602 (2008).
- [61] K. V. Krutitsky, *Ultracold bosons with short-range interaction in regular optical lattices*, *Phys. Rep.* **607**, 1 (2016).
- [62] S. D. Huber, E. Altman, H. P. Büchler, and G. Blatter, *Dynamical properties of ultracold bosons in an optical lattice*, *Phys. Rev. B* **75**, 085106 (2007).
- [63] S. M. Davidson and A. Polkovnikov, *SU(3) Semiclassical Representation of Quantum Dynamics of Interacting Spins*, *Phys. Rev. Lett.* **114**, 045701 (2015).
- [64] V. Murg, F. Verstraete, and J. I. Cirac, *Variational study of hardcore bosons in a two-dimensional optical lattice using projected entangled pair states*, *Phys. Rev. A* **75**, 033605 (2007).
- [65] J. Jordan, R. Orús, and G. Vidal, *Numerical study of the hardcore Bose-Hubbard model on an infinite square lattice*, *Phys. Rev. B* **79**, 174515 (2009).
- [66] A. Kshetrimayum, M. Rizzi, J. Eisert, and R. Orús, *Tensor Network Annealing Algorithm for Two-Dimensional Thermal States*, *Phys. Rev. Lett.* **122**, 070502 (2019).
- [67] S. S. Jahromi and R. Orús, *Universal tensor-network algorithm for any infinite lattice*, *Phys. Rev. B* **99**, 195105 (2019).
- [68] S. S. Jahromi and R. Orús, *Thermal bosons in 3d optical lattices via tensor networks*, *Sci. Rep.* **10**, 19051 (2020).
- [69] P. Schmoll, S. S. Jahromi, M. Hörmann, M. Mühlhauser, K. P. Schmidt, and R. Orús, *Fine Grained Tensor Network Methods*, *Phys. Rev. Lett.* **124**, 200603 (2020).

- [70] W.-L. Tu, H.-K. Wu, and T. Suzuki, *Frustration-induced super-solid phases of extended Bose-Hubbard model in the hard-core limit*, *J. Phys.: Cond. Mat.* **32**, 455401 (2020).
- [71] H.-K. Wu and W.-L. Tu, *Competing quantum phases of hard-core bosons with tilted dipole-dipole interaction*, *Phys. Rev. A* **102**, 053306 (2020).
- [72] P. C. G. Vlaar and P. Corboz, *Simulation of three-dimensional quantum systems with projected entangled-pair states*, *Phys. Rev. B* **103**, 205137 (2021).
- [73] H. F. Trotter, *On the product of semi-groups of operators*, *Proc. Amer. Math. Soc.* **10**, 545 (1959).
- [74] M. Suzuki, *Pair-product model of Heisenberg ferromagnets*, *J. Phys. Soc. Jpn.* **21**, 2274 (1966).
- [75] M. Suzuki, *Relationship between d -dimensional quantal spin systems and $(d+1)$ -dimensional ising systems: Equivalence, critical exponents and systematic approximants of the partition function and spin correlations*, *Prog. Theor. Phys.* **56**, 1454 (1976).
- [76] H. C. Jiang, Z. Y. Weng, and T. Xiang, *Accurate Determination of Tensor Network State of Quantum Lattice Models in Two Dimensions*, *Phys. Rev. Lett.* **101**, 090603 (2008).
- [77] Y. Motoyama, T. Okubo, K. Yoshimi, S. Morita, T. Kato, and N. Kawashima, *TeNeS: Tensor Network Solver for Quantum Lattice Systems*, [arXiv:2112.13184](https://arxiv.org/abs/2112.13184).
- [78] TeNeS: <https://github.com/issp-center-dev/TeNeS>.
- [79] pTNS: <https://github.com/TsuyoshiOkubo/pTNS>.
- [80] T. Nishino and K. Okunishi, *Corner Transfer Matrix Renormalization Group Method*, *J. Phys. Soc. Jpn.* **65**, 891 (1996).
- [81] T. Nishino and K. Okunishi, *Corner transfer matrix algorithm for classical renormalization group*, *J. Phys. Soc. Jpn.* **66**, 3040 (1997).
- [82] T. Nishino, T. Hikihara, K. Okunishi, and Y. Hieida, *Density matrix renormalization group: Introduction from a variational point of view*, *Int. J. Mod. Phys. B* **13**, 1 (1999).
- [83] R. Orús and G. Vidal, *Simulation of two-dimensional quantum systems on an infinite lattice revisited: Corner transfer matrix for tensor contraction*, *Phys. Rev. B* **80**, 094403 (2009).
- [84] P. Corboz, J. Jordan, and G. Vidal, *Simulation of fermionic lattice models in two dimensions with projected entangled-pair states: Next-nearest neighbor Hamiltonians*, *Phys. Rev. B* **82**, 245119 (2010).
- [85] P. Corboz, S. R. White, G. Vidal, and M. Troyer, *Stripes in the two-dimensional t - J model with infinite projected entangled-pair states*, *Phys. Rev. B* **84**, 041108(R) (2011).
- [86] P. Corboz, T. M. Rice, and M. Troyer, *Competing States in the t - J Model: Uniform d -Wave State versus Stripe State*, *Phys. Rev. Lett.* **113**, 046402 (2014).

ACKNOWLEDGMENTS

We acknowledge fruitful discussions with S. Goto and K. Nagao. We thank Y. Takahashi and Y. Takasu for useful discussions and the experimental data. This work was financially supported by JSPS KAKENHI (Grants Nos. JP18H05228, JP21H01014, and JP21K13855), by JST CREST (Grant No. JPMJCR1673), by JST FOREST (Grant No. JPMJFR202T), and by MEXT Q-LEAP (Grant No. JPMXS0118069021). The numerical computations were performed on computers at the Yukawa Institute Computer Facility and on computers at the Supercomputer Center, the Institute for Solid State Physics, the University of Tokyo.

VII. AUTHOR CONTRIBUTIONS

R.K. and I.D. designed and coordinated the studies. R.K. performed the numerical simulations. R.K. and I.D. contributed to the writing of the paper.

VIII. COMPETING INTERESTS

The authors declare no competing interests.

IX. ADDITIONAL INFORMATION

Supplementary Information The online version contains supplementary material available at <https://doi.org/10.1038/s42005-022-00848-9>.

Supplementary Information: Tensor-network study of correlation-spreading dynamics in the two-dimensional Bose-Hubbard model

Ryui Kaneko* and Ippei Danshita†

Department of Physics, Kindai University, Higashi-Osaka, Osaka 577-8502, Japan

(Dated: March 23, 2022)

CONTENTS

Supplementary Note 1: Time dependence of the hopping and the interaction during a finite-time quench	1
Supplementary Note 2: Further comparison with the exact diagonalization for a sudden quench to stronger interaction	1
Supplementary Note 3: Further comparison with the exact diagonalization for a sudden quench to weaker interaction	2
Supplementary Note 4: Further comparison with the experiment for a finite-time quench	2
Supplementary Note 5: Comparison with the truncated Wigner approximation for a finite-time quench	3
Supplementary Note 6: Time dependence of energy in the moderate interaction region	3
Supplementary Note 7: Single-particle and density-density correlation functions for several interaction parameters	3
Supplementary Note 8: Extraction of propagation velocities in the moderate interaction region	5
Supplementary Note 9: Extraction of propagation velocities for much stronger interaction	6
Supplementary Note 10: Choice of the dimension of the local Hilbert space	7
Supplementary References	7

Supplementary Note 1: TIME DEPENDENCE OF THE HOPPING AND THE INTERACTION DURING A FINITE-TIME QUENCH

We briefly review the detailed setup in the experiment [S1] and the time dependence of the hopping and the interaction. In the experiment, ultracold Bose gas of ^{174}Yb atoms is confined in the optical lattice with the lattice spacing $d_{\text{lat}} = 266\text{nm}$.

At the time $t = -\tau_Q = -0.1\text{ms}$, the Mott insulator at $\nu = 1$ is prepared in the optical lattice with the depth $V_0 = 15E_R$. The interaction and the hopping are $U(V_0 = 15E_R) \sim 0.648E_R$ and $J(V_0 = 15E_R) \sim 0.00652E_R$, respectively, and their ratio is $U/J \sim 99.4$. Here $E_R/(2\pi\hbar) = 4021.18\text{Hz}$ is the recoil energy of the system.

For $-\tau_Q < t < 0$, the lattice depth is decreased rapidly to $V_0 = 9E_R$. The change of the depth is nearly a linear function of time, namely, $V_0(t)/E_R = 9 - 6t/\tau_Q$. Finally, the interaction and the hopping become $U(V_0 = 9E_R) \sim 0.474E_R$ and $J(V_0 = 9E_R) \sim 0.0242E_R$, respectively. Their ratio becomes $U/J \sim 19.6$, which corresponds to the Mott insulating region close to the critical point $U_c/J \sim 16.7$ [S2–S4]. In the iPEPS simulations, we take $J_{\text{final}} = J(V_0 = 9E_R)$ as the unit of energy. The corresponding unit of timescale is $\tau_{\text{unit}} = \hbar/J_{\text{final}} \sim 1.63\text{ms}$, and the length of the quench time is expressed as $\tau_Q = 0.1\text{ms} \sim 0.0612\tau_{\text{unit}}$.

For $t > 0$, the hopping and the interaction are fixed. The single-particle correlation functions are obtained by measuring the time-of-flight interference pattern.

All the time dependence of the hopping $J(t)$ and the interaction $U(t)$ are summarized in Fig. S1.

Supplementary Note 2: FURTHER COMPARISON WITH THE EXACT DIAGONALIZATION FOR A SUDDEN QUENCH TO STRONGER INTERACTION

To examine to what extent the energy is conserved in the case of a sudden quench at $U/J = 19.6$, we calculate the time dependence of the grand potential density at $T = 0$ obtained by iPEPS in Fig. S2. It is nearly constant ($e_{\text{MI}}/J = -\tilde{\mu}U/J$ with $\tilde{\mu} = \mu/U = -0.371$ [S2–S4]) for $t \lesssim 0.4\hbar/J$. The data almost converge for the bond dimensions $D \geq 6$ in this short time.

We also compare the single-particle correlation functions at a far distance $|\mathbf{r}| = 2$ obtained by iPEPS with those obtained by ED in Fig. S3. In contrast to the ED data at distances $|\mathbf{r}| = 1$ and $|\mathbf{r}| = \sqrt{2}$, they do not converge for the system sizes $N_s \leq 20$. This is because a distance $|\mathbf{r}| = 2$ reaches a half the length of the lattice, and consequently, the boundary effect is significant. The data of iPEPS simulations, in which

* rkaneko@phys.kindai.ac.jp

† danshita@phys.kindai.ac.jp

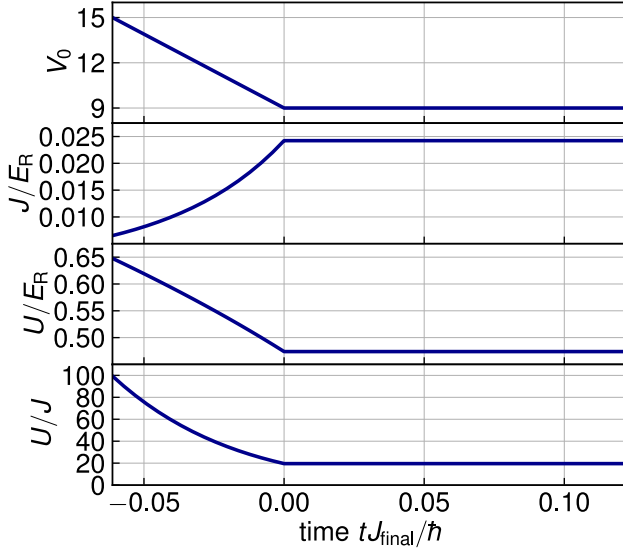


FIG. S1. Time dependence of the depth V_0 of the optical lattice, the hopping J/E_R , the interaction U/E_R , and the ratio U/J . The recoil energy is $E_R/(2\pi\hbar) = 4021.18\text{Hz}$.

the quantities at the thermodynamic limit are obtained directly, converge very well for $D \geq 6$. The first peaks in the ED simulations gradually converge to those in the iPEPS simulations as the system size increases. This observation suggests that the iPEPS result represents the correlation functions in the thermodynamic limit fairly well.

Supplementary Note 3: FURTHER COMPARISON WITH THE EXACT DIAGONALIZATION FOR A SUDDEN QUENCH TO WEAKER INTERACTION

To demonstrate the applicability of the iPEPS method for a relatively weaker interaction region, we also compare the single-particle correlation functions obtained by the iPEPS and ED methods. As examples, we show the correlation functions for $U/J = 10$ and 4.

For $U/J = 10$, the ED results show relatively large size dependence for $N_s \leq 16$ (see Fig. S4). The iPEPS results are well converged for $D \geq 7$. The data obtained by iPEPS and those by ED for $N_s = 16$ overlap very well within a short time frame ($tJ/\hbar \lesssim 0.3$).

On the other hand, for $U/J = 4$, the ED results are nearly converged for $N_s \geq 9$ (see Fig. S5). Likewise, the iPEPS results are nearly converged for $D \geq 8$ when $tJ/\hbar \lesssim 0.6$. As in the case of $U/J = 10$, the data obtained by iPEPS for $D = 9$ and those by ED overlap very well for $tJ/\hbar \lesssim 0.8$.

Supplementary Note 4: FURTHER COMPARISON WITH THE EXPERIMENT FOR A FINITE-TIME QUENCH

As in the sudden quench case, we show the time dependence of the grand potential density at $T = 0$ obtained by iPEPS in the case of a finite-time quench at $U/J_{\text{final}} = 19.6$ in Fig. S6.

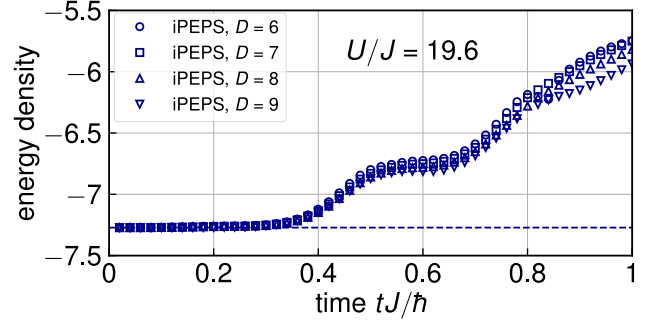


FIG. S2. Time dependence of the grand potential density in the unit of hopping energy J for a sudden quench at $U/J = 19.6$. The energy density at $t = 0$ is given as a dashed line. The energy density is nearly conserved in a short time $t \lesssim 0.4\hbar/J$.

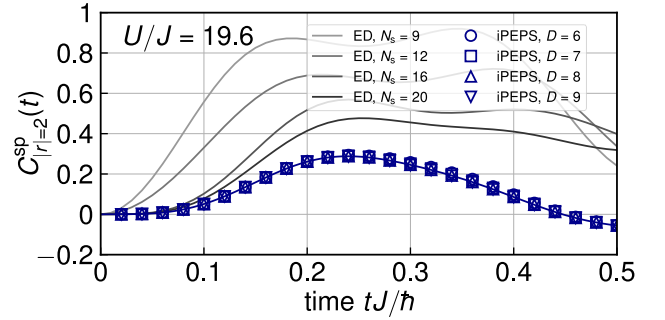


FIG. S3. Comparison of the single-particle correlation functions in the case of a sudden quench between iPEPS (blue lines with symbols) and ED (gray lines). The correlations at a distance $|r| = 2$ is shown.

For $-\tau_Q < t < 0$, both parameters U and J are controlled, and the energy also varies. At $t = -\tau_Q$, it is $e_{\text{MI}}(t = -\tau_Q)/J_{\text{final}} = -\tilde{\mu}U(t = -\tau_Q)/J_{\text{final}} \sim -0.371 \times 26.7 \sim -9.91$. On the other hand, for $t > 0$, it is $e_{\text{MI}}(t > 0)/J_{\text{final}} \sim -0.371 \times 19.6 \sim -7.27$ as in the case of the sudden quench. The energy density is nearly conserved for $t \lesssim 0.4\hbar/J_{\text{final}}$.

In the experiment [S1], the correlation functions along the horizontal [$\mathbf{r} = (x, 0)$] and vertical [$\mathbf{r} = (0, y)$] directions are observed separately. We have compared the results for $\mathbf{r} = (0, y)$ in the main text. Here we show the results for $\mathbf{r} = (x, 0)$ (see Fig. S7). The intensities along the horizontal direction are slightly smaller than those along the vertical direction in the experiment. Nevertheless, the intensity obtained by iPEPS is almost consistent with that in the experiment. The first-peak times for $|r| = 1, 2$, and 3 obtained by iPEPS also agree very well with the experimental results.

We also compare the single-particle correlation function at a distance $|r| = \sqrt{2}$ in Fig. S8. The first-peak times are nearly the same between the experiment and iPEPS simulations. However, the intensity obtained by iPEPS is nearly 1.5 times larger than that in the experiment, and the difference is at more than a few-sigma level. Note that the intensity of correlations at a distance $|r| = \sqrt{2}$ by iPEPS overlaps perfectly with those by ED (see the main text) and by TWA (see the next section) within the time shorter than $\sim 0.2\hbar/J_{\text{final}}$. At the moment, we do not know the origin of the difference between

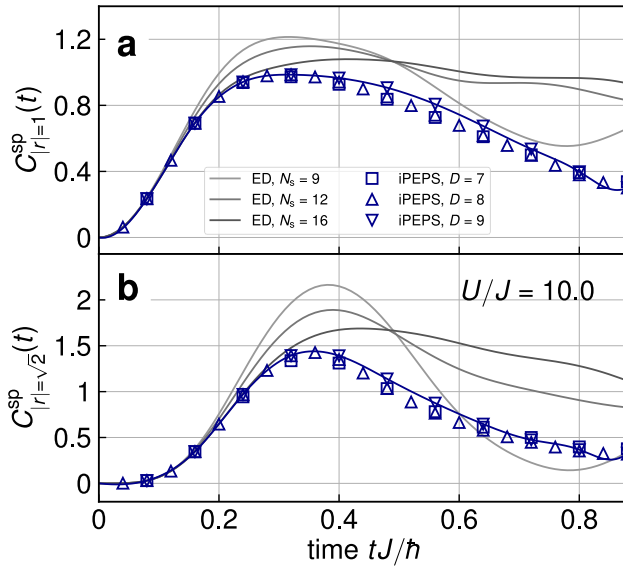


FIG. S4. Comparison of the single-particle correlation functions in the case of a sudden quench between iPEPS (blue lines with symbols) and ED (gray lines) for $U/J = 10$.

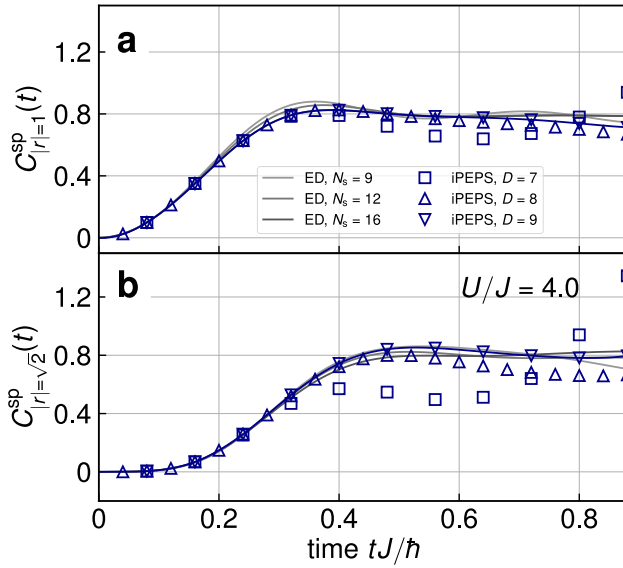


FIG. S5. Comparison of the single-particle correlation functions in the case of a sudden quench between iPEPS (blue lines with symbols) and ED (gray lines) for $U/J = 4$.

the experimental and theoretical results.

Supplementary Note 5: COMPARISON WITH THE TRUNCATED WIGNER APPROXIMATION FOR A FINITE-TIME QUENCH

We compare the single-particle correlation functions of iPEPS and TWA [S5] in the case of a finite-time quench in Fig. S9. When $|r| = 1$, in a short time $t \lesssim 0.1\hbar/J_{\text{final}}$, the results of iPEPS, Gaussian SU(3)TWA, and discrete SU(3)TWA

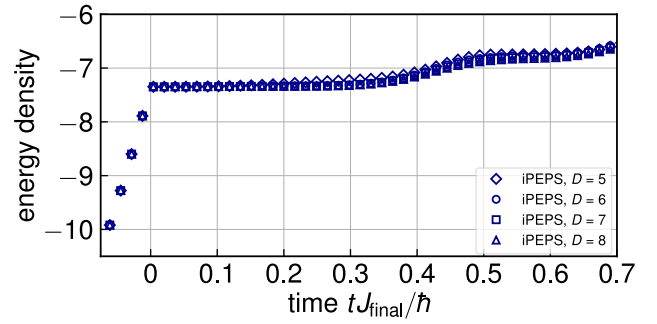


FIG. S6. Time dependence of the grand potential density in the unit of hopping energy J_{final} for a finite-time quench at $U/J_{\text{final}} = 19.6$. The energy density is nearly conserved in a short time $0 < t \lesssim 0.4\hbar/J_{\text{final}}$.

[SU(3)DTWA] agree very well, whereas the intensity obtained by the Gross-Pitaevskii TWA (GPTWA) is slightly smaller. On the other hand, the first-peak time of iPEPS agrees very well with that of GPTWA, whereas the peaks of Gaussian SU(3)TWA and SU(3)DTWA are very broad. Remarkably, when $|r| = \sqrt{2}$ and $|r| = 2$, in a short time slightly before the appearance of the first peak in iPEPS simulations, the results of iPEPS and Gaussian SU(3)TWA overlap perfectly. The intensity obtained by SU(3)DTWA (GPTWA) is slightly larger (much smaller) than that obtained by iPEPS. As in the case of $|r| = 1$, the first peaks of SU(3)TWA and SU(3)DTWA are broad, and it is hard to extract the correct first-peak times from these TWA data. For $|r| = 2$, the first-peak times obtained by SU(3)TWA and SU(3)DTWA are longer than those estimated from the experiment and iPEPS. The iPEPS can simulate real-time dynamics in a slightly longer time and capture the first-peak structures more clearly.

Supplementary Note 6: TIME DEPENDENCE OF ENERGY IN THE MODERATE INTERACTION REGION

Figure S10 shows the time dependence of the grand potential density at each U/J . When $U/J \sim 10$, the energy gradually increases with increasing time. This tendency is similar to what we have found at $U/J = 19.6$. By contrast, when $U/J \sim 2$, the energy decreases with increasing time. In the intermediate region, especially for $U/J \sim 5$, the behavior of energy going up and going down cancel each other out. Remarkably, it is conserved for $t \lesssim 0.9\hbar/J$, much longer than the time at $U/J = 19.6$. This indicates that the real-time evolution can be simulated in a longer time in the moderate interaction region.

Supplementary Note 7: SINGLE-PARTICLE AND DENSITY-DENSITY CORRELATION FUNCTIONS FOR SEVERAL INTERACTION PARAMETERS

To investigate the propagation velocities, we use the single-particle and density-density correlation functions. Here we demonstrate how they behave for small and large interaction

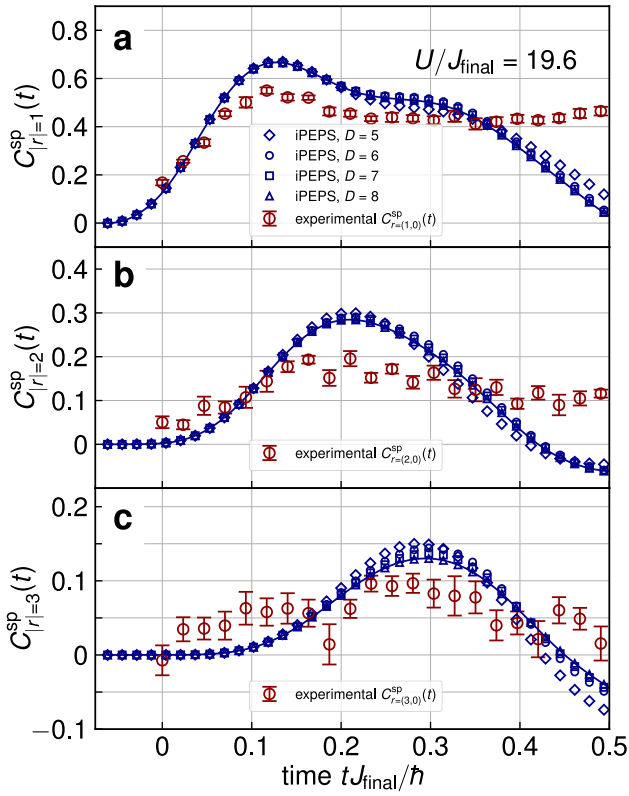


FIG. S7. Comparison of the single-particle correlation functions in the case of a finite-time quench between iPEPS (blue lines with symbols) and the experiment (red circles with error bars). The correlations at distances (a) $|r| = 1$, (b) $|r| = 2$, and (c) $|r| = 3$ are shown. Here the experimental results for $r = (x, y)$ are given, while those for $r = (0, y)$ are given in the main text.

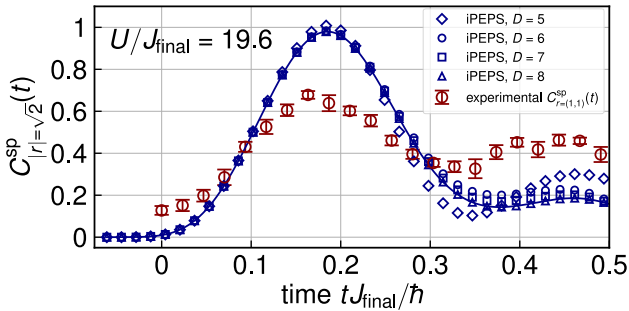


FIG. S8. Comparison of the single-particle correlation functions in the case of a finite-time quench between iPEPS (blue lines with symbols) and the experiment (red circles with error bars). The correlations at a distance $|r| = \sqrt{2}$ is shown.

regions.

When the interaction is small ($U/J = 2$), it is difficult to follow the correlation peaks in the single-particle correlation functions within accessible simulation time, as shown in Fig. S11(a). The first peak at $|r| = 1$ is broad, while peaks do not appear at $|r| = \sqrt{2}, 2$, and 3 for $t \lesssim 0.9\hbar/J$. This behavior persists until $U/J \sim 4$. Because of the lack of data points of correlation peaks, we can extract the phase velocities only

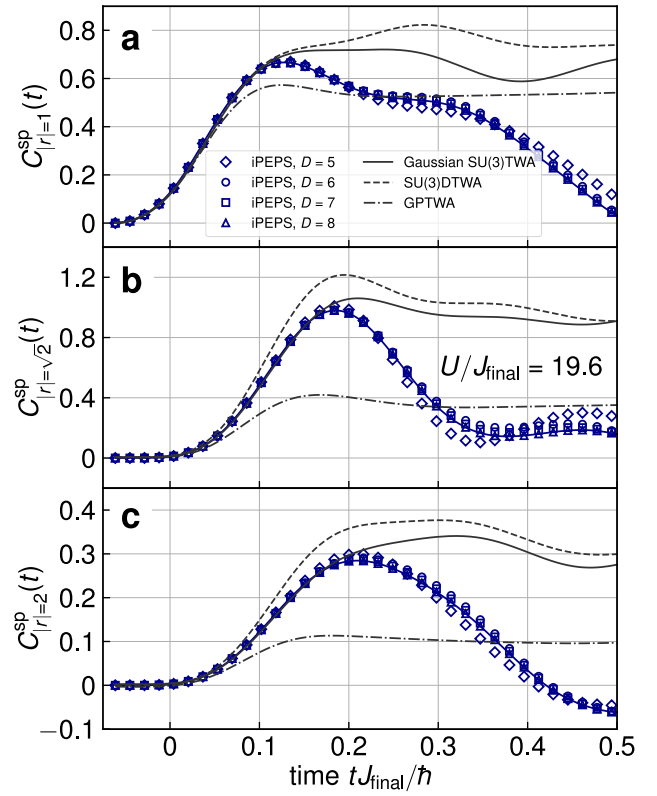


FIG. S9. Comparison of the single-particle correlation functions in the case of a finite-time quench between iPEPS (blue lines with symbols) and TWA (gray lines). The correlations at distances (a) $|r| = 1$, (b) $|r| = \sqrt{2}$, and (c) $|r| = 2$ are shown. Results of iPEPS and Gaussian SU(3)TWA are in good agreement in a short time slightly before the appearance of the first peaks obtained by iPEPS.

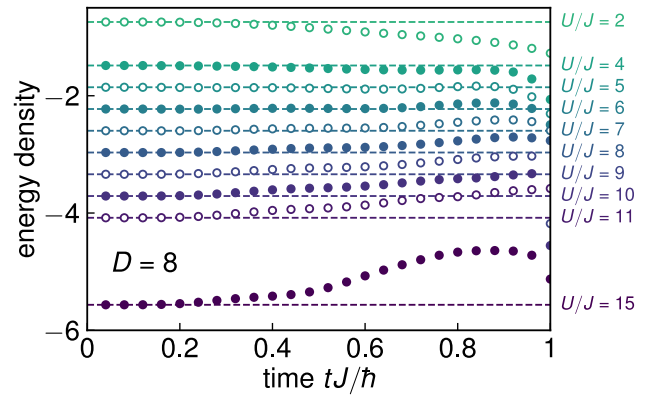


FIG. S10. Time dependence of the grand potential density in the unit of hopping energy J for a sudden quench at each U/J . The energy densities at $t = 0$ are given as dashed lines. When $U/J \sim 5$, the energy density is nearly conserved for a rather longer time $t \lesssim 0.9\hbar/J$.

for $U/J \geq 5$. On the other hand, we observe clear first peaks in the density-density correlation functions [see Fig. S11(b)]. The first-peak times are nearly consistent with those obtained by TWA at high filling $\nu = 10$ [S6].

When the interaction is strong ($U/J = 19.6$), we success-

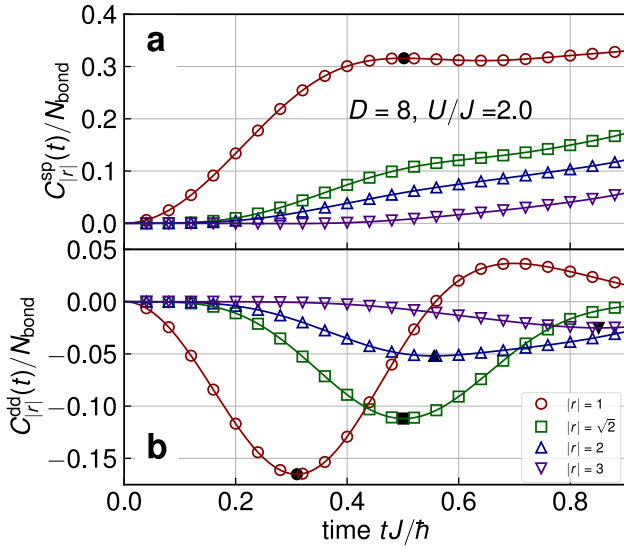


FIG. S11. (a) Single-particle and (b) density-density correlation functions per bond at $U/J = 2$ for the bond dimension $D = 8$.

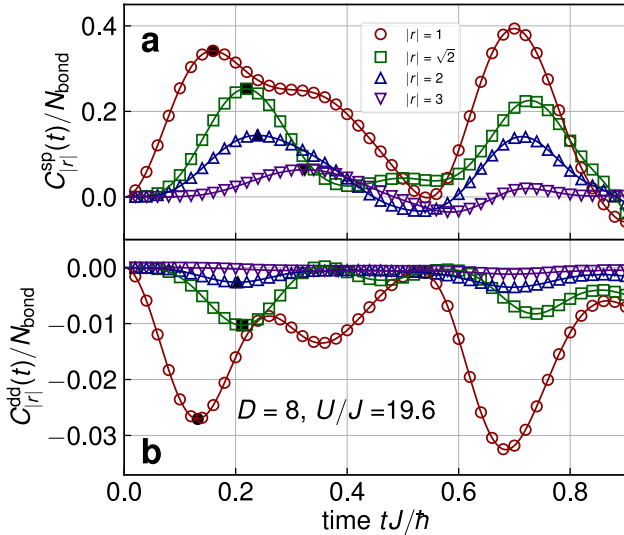


FIG. S12. (a) Single-particle and (b) density-density correlation functions per bond at $U/J = 19.6$ for the bond dimension $D = 8$.

fully capture all the first peaks up to $|r| \leq 3$ within the reliable simulation time $t \lesssim 0.4\hbar/J$ (see Fig. S12). The maximum intensity in the single-particle correlation function ($\max |C_{|r|}^{sp}(t)/N_{bond}| \sim 0.35$) is comparable to that for the small interaction [compare Figs. S11(a) and S12(a)]. By contrast, the maximum intensity of the density-density correlation function ($\max |C_{|r|}^{dd}(t)/N_{bond}| \sim 0.03$) is much smaller than that for the small interaction [compare Figs. S11(b) and S12(b)]. The particle fluctuation is strongly suppressed in the large U region, and the peak intensity decays rapidly as a function of a distance.

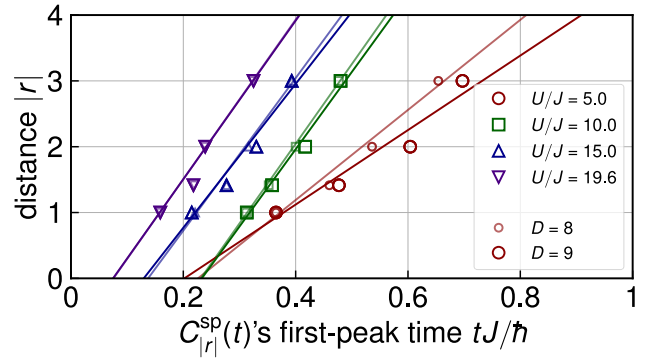


FIG. S13. Peak-time dependence of distance obtained from the single-particle correlation functions for $D = 8$ and $D = 9$.

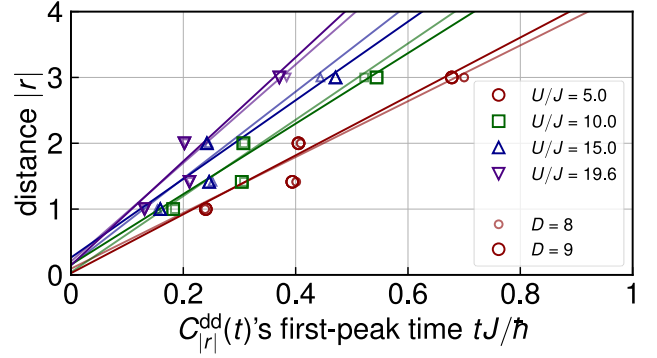


FIG. S14. Peak-time dependence of distance obtained from the density-density correlation functions for $D = 8$ and $D = 9$.

Supplementary Note 8: EXTRACTION OF PROPAGATION VELOCITIES IN THE MODERATE INTERACTION REGION

We show the peak-time dependence of distance obtained from the single-particle correlation functions $C_{|r|}^{sp}(t)$ in Fig. S13. For all the values of U/J that we have taken in our analyses, the first-peak times of the correlations at $|r| = 3$ are well below the time when the energy density is no longer conserved (see Fig. S10). At $U/J = 5$, the data points for the bond dimensions $D = 8$ and $D = 9$ deviate a little. On the other hand, for $U/J \geq 10$, they are nearly the same and are well converged. The phase velocity along the horizontal or vertical axis is estimated by fitting data points at $|r| = 1, 2$, and 3. The slopes are found to be nearly the same for $D = 8$ and $D = 9$.

We also show the peak-time dependence of distance obtained from the density-density correlation functions $C_{|r|}^{dd}(t)$ in Fig. S14. In this case, the first-peak times of the correlations at $|r| = 3$ is comparable to or slightly less than the time when the energy density is no longer conserved (see Fig. S10). Therefore, data points up to $|r| = 3$ reach near the limit of what we can do in our iPEPS simulations. For all U/J , the data points for $D = 8$ and $D = 9$ are similar. The group velocity along the horizontal or vertical axis is estimated by fitting data points at $|r| = 1, 2$, and 3.

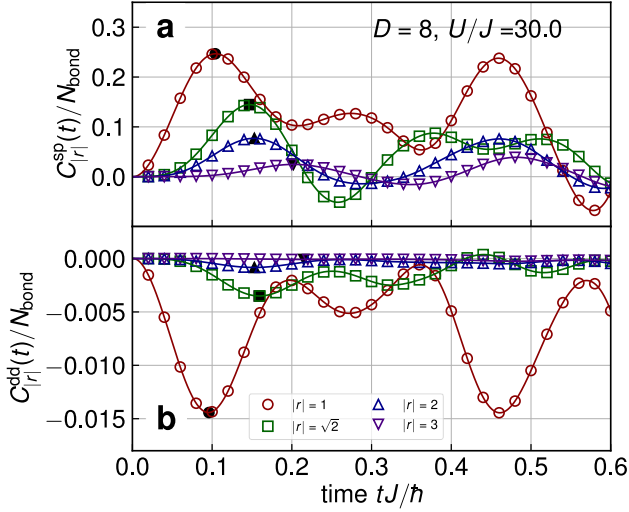


FIG. S15. (a) Single-particle and (b) density-density correlation functions per bond at $U/J = 30$ for the bond dimension $D = 8$.

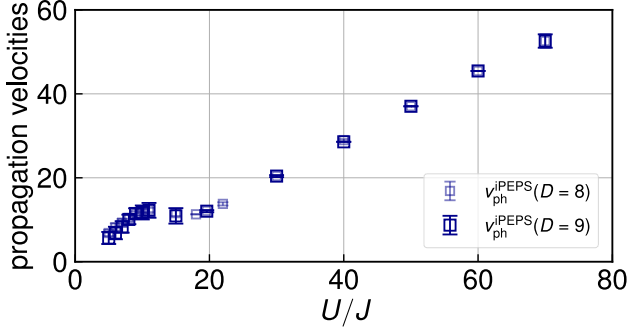


FIG. S16. Estimated phase velocity from the single-particle correlation functions for the bond dimensions $D = 8$ and $D = 9$.

Note that the peak at $|r| = \sqrt{2}$ does not have to be on the line connecting data points at $|r| = 1, 2$, and 3 . As discussed in Refs. [S1, S7–S9], the correlation spreading in 2D can be highly anisotropic in general. As for the low-energy physics, dynamics of the system is dominated by long wavelength excitations, and the correlation front propagates according to the Euclidean metrics. However, when the system is quenched, various wavelengths are mixed. In this situation, short wavelength excitations also participate, and the Manhattan metrics are more relevant to the propagation of the correlation front. Reflecting this fact, the first peaks of the correlation functions for $|r| = 2$ and $|r| = \sqrt{2}$, having the same Manhattan distance, appear nearly simultaneously (see Fig. S14).

Estimated group and phase velocities for $2 \leq U/J \leq 22$ are summarized in the main text.

Supplementary Note 9: EXTRACTION OF PROPAGATION VELOCITIES FOR MUCH STRONGER INTERACTION

As for much stronger interaction, we successfully estimate the phase velocity using the correlation functions obtained by

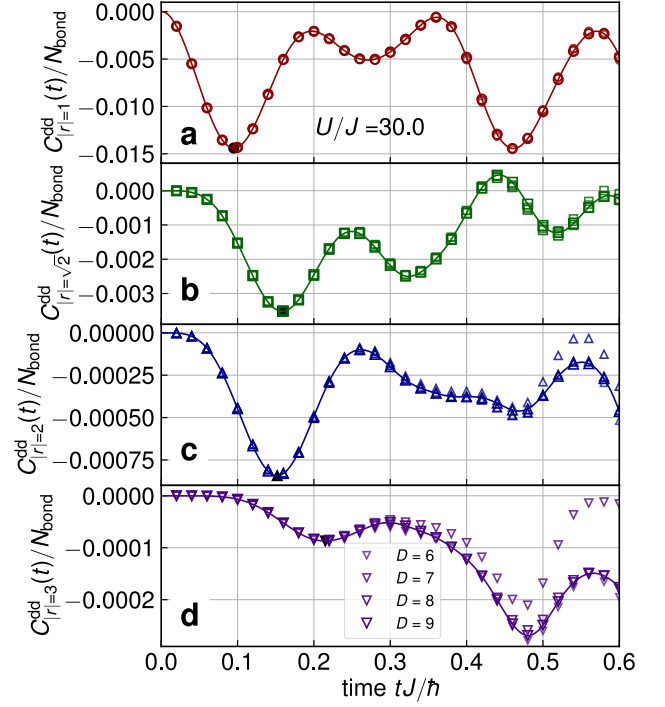


FIG. S17. Density-density correlation functions per bond at $U/J = 30$ that are the same as those in Fig. S15, but the vertical axes are magnified.

the iPEPS simulations. On the other hand, it is much harder to extract the group velocity. In this section, we summarize our results for much stronger interaction.

As in the moderate interaction region, we extract the phase velocity from the single-particle correlation functions. They behave similarly between the moderate and stronger interaction regions although each first-peak time of the single-particle correlation shifts to an earlier time as interaction increases (compare, for example, Fig. S12 and Fig. S15). From the first-peak-time dependence of distance, we extract the phase velocity as shown in Fig. S16. The phase velocity is dominated by the energy scale of interaction and is nearly a linear function of U/J . The estimated value $v_{ph} \sim 30J/\hbar$ at $U/J \sim 40$ is comparable to the value obtained by the 2PISC method in Ref. [S7].

On the other hand, within the accessible simulation time, we are not able to extract the group velocity for very large U/J . The group and phase velocities start to deviate even when we use the density-density correlation functions to extract the group velocity. To accurately estimate the group velocity, which is slower than the phase velocity, we have to carefully follow the envelope of the correlation function for slightly longer time. To examine how the envelope should look like, we plot the typical behavior of the density-density correlation functions for $U/J = 30$ in Fig. S17. When we focus on the correlation function at $|r| = 3$, the first-peak time is located at $tJ/\hbar \sim 0.2$. On the other hand, because this peak $|C_{|r|=3}^{dd}(tJ/\hbar \sim 0.2)|$ seems to be smaller than the second peak at $tJ/\hbar \sim 0.5$, it is likely that the peak of the true envelope of

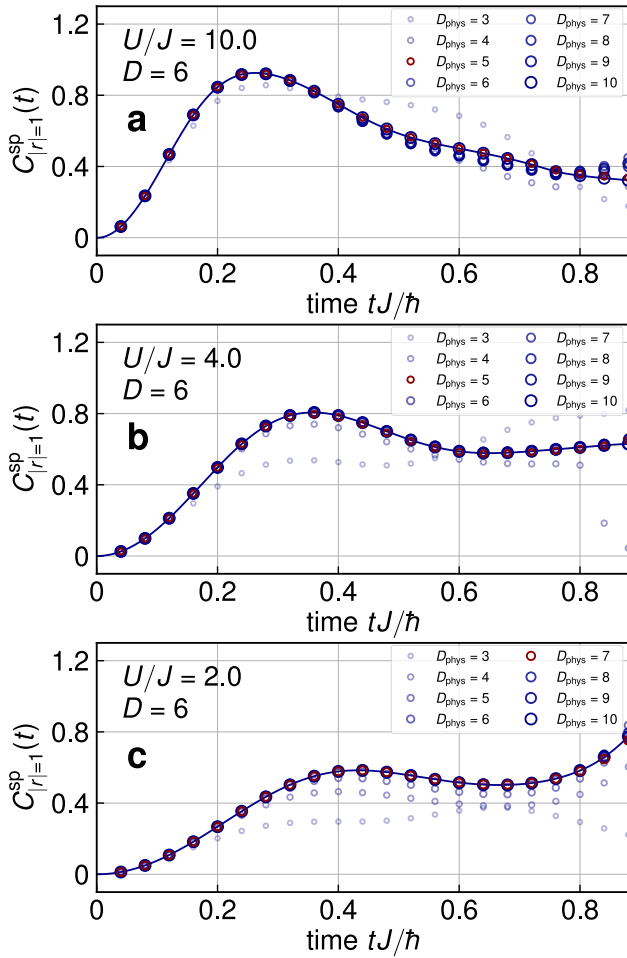


FIG. S18. Single-particle correlation functions as functions of the dimension of the local Hilbert space D_{phys} for (a) $U/J = 10$, (b) $U/J = 4$, and (c) $U/J = 2$.

the correlation function is at the later time than $tJ/\hbar \sim 0.2$. However, because the energy is nearly conserved up to a short time $tJ/\hbar \sim 0.4$, it is not possible to estimate the peak of the envelope, which should be determined by connecting at least three peak points.

Supplementary Note 10: CHOICE OF THE DIMENSION OF THE LOCAL HILBERT SPACE

To determine the appropriate dimension of the local Hilbert space D_{phys} , we calculate correlation functions up to $D_{\text{phys}} = 10$ for several interaction parameters. For a quench to the Mott insulating region, choosing $D_{\text{phys}} = 3$ reproduces the experi-

mental and other numerical results very well. Here we focus on a quench to the superfluid parameter region. Because qualitative behavior of correlation functions is nearly converged for $D \geq 6$, we examine the D_{phys} dependence at $D = 6$. We show the D_{phys} dependence of the single-particle correlation functions for selected interaction parameters in Fig. S18. (The density-density correlation functions and correlation functions for $|r| > 1$ also behave in a qualitatively similar manner and are not shown here.)

For $U/J = 10$, the first-peak time is nearly identical for $D_{\text{phys}} \geq 3$. The correlation functions nearly converge to the same curve for $D_{\text{phys}} \geq 4$. Even if we lower the interaction strength to $U/J = 4$, the correlation functions appear to converge very well for $D_{\text{phys}} \geq 5$. Therefore, we have chosen $D_{\text{phys}} = 5$ for $U/J \geq 4$.

On the other hand, for $U/J = 2$, the correlation function for $D_{\text{phys}} = 5$ is slightly smaller than the converged curve. Although the data for $D_{\text{phys}} = 5$ and those for $D_{\text{phys}} > 5$ are not so different, we have chosen $D_{\text{phys}} = 7$ particularly for $U/J = 2$ to maximize safety.

SUPPLEMENTARY REFERENCES

- [S1] Y. Takasu, T. Yagami, H. Asaka, Y. Fukushima, K. Nagao, S. Goto, I. Danshita, and Y. Takahashi, *Energy redistribution and spatio-temporal evolution of correlations after a sudden quench of the Bose-Hubbard model*, *Sci. Adv.* **6**, eaba9255 (2020).
- [S2] N. Elstner and H. Monien, *Dynamics and thermodynamics of the Bose-Hubbard model*, *Phys. Rev. B* **59**, 12184 (1999).
- [S3] B. Capogrosso-Sansone, Ş. G. Söyler, N. Prokof'ev, and B. Svistunov, *Monte Carlo study of the two-dimensional Bose-Hubbard model*, *Phys. Rev. A* **77**, 015602 (2008).
- [S4] K. V. Krutitsky, *Ultracold bosons with short-range interaction in regular optical lattices*, *Phys. Rep.* **607**, 1 (2016).
- [S5] K. Nagao, Y. Takasu, Y. Takahashi, and I. Danshita, *SU(3) truncated Wigner approximation for strongly interacting Bose gases*, *Phys. Rev. Research* **3**, 043091 (2021).
- [S6] K. Nagao, M. Kunimi, Y. Takasu, Y. Takahashi, and I. Danshita, *Semiclassical quench dynamics of Bose gases in optical lattices*, *Phys. Rev. A* **99**, 023622 (2019).
- [S7] A. Mokhtari-Jazi, M. R. C. Fitzpatrick, and M. P. Kennett, *Phase and group velocities for correlation spreading in the Mott phase of the Bose-Hubbard model in dimensions greater than one*, *Phys. Rev. A* **103**, 023334 (2021).
- [S8] G. Carleo, F. Becca, L. Sanchez-Palencia, S. Sorella, and M. Fabrizio, *Light-cone effect and supersonic correlations in one- and two-dimensional bosonic superfluids*, *Phys. Rev. A* **89**, 031602(R) (2014).
- [S9] L. Cevolani, J. Despres, G. Carleo, L. Tagliacozzo, and L. Sanchez-Palencia, *Universal scaling laws for correlation spreading in quantum systems with short- and long-range interactions*, *Phys. Rev. B* **98**, 024302 (2018).